A delayed action oscillator shared by biennial, interannual, and decadal signals in the Pacific Basin

Warren B. White,[1] Yves M. Tourre,[2] Mathew Barlow,[3] and Mike Dettinger[4]

Received 24 May 2002; revised 31 October 2002; accepted 20 November 2002; published 13 March 2003.

[1] Biennial, interannual, and decadal signals in the Pacific basin are observed to share patterns and evolution in covarying sea surface temperature (SST), 18°C isotherm depth (Z18), zonal surface wind (ZSW), and wind stress curl (WSC) anomalies from 1955 to 1999. Each signal has warm SST anomalies propagating slowly eastward along the equator, generating westerly ZSW anomalies in their wake. These westerly ZSW anomalies produce cyclonic WSC anomalies off the equator which pump baroclinic Rossby waves in the western/central tropical North Pacific Ocean. These Rossby waves propagate westward, taking ~6, ~12, and ~36 months to reach the western boundary near ~7°N, ~12°N, and ~18°N on biennial, interannual, and decadal period scales, respectively. There, they reflect as equatorial coupled waves, propagating slowly eastward in covarying SST, Z18, and ZSW anomalies, taking ~6, ~12, and ~24 months to reach the central/eastern equatorial ocean. These equatorial coupled waves produce a delayed-negative feedback to the warm SST anomalies there. The decrease in Rossby wave phase speed with latitude, the increase in meridional scale of equatorial SST anomalies with period scale, and the associated increase in latitude of Rossby wave forcing are consistent with the delayed action oscillator (DAO) model used to explain El Niño. However, this is not true of the western-boundary reflection of Rossby waves into slow equatorial coupled waves. This requires modification of the extant DAO model. We construct a modified DAO model, demonstrating how the various mechanisms and the size and sources of their delays yield the resulting frequency of each signal. *INDEX TERMS:* 4522 Oceanography: Physical: El Niño; 4572 Oceanography: Physical: Upper ocean processes; 4576 Oceanography: Physical: Western boundary currents; 4299 Oceanography: General: General or miscellaneous; *KEYWORDS:* Pacific biennial signals, Pacific interannual signals, Pacific decadal signals, coupling physics of decadal signals

Citation: White, W. B., Y. M. Tourre, M. Barlow, and M. Dettinger, A delayed action oscillator shared by biennial, interannual, and decadal signals in the Pacific Basin, *J. Geophys. Res.*, *108*(C3), 3070, doi:10.1029/2002JC001490, 2003.

1. Introduction

[2] *Allan* [2000], *White and Cayan* [2000], and *Tourre et al.* [2001] computed spectra for sea surface temperature (SST) and sea level pressure (SLP) anomalies over the Indo-Pacific Ocean for the past 100 years, finding significant peaks for biennial (2.2- and 2.8-year) signals, interannual (3.5-, 5.4-, and 7-year) signals, and a decadal (11-year) signal. These quasiperiodic signals are similar to those observed by *Mann and Park* [1996] and *Lau and Weng* [1995] in covarying surface temperature and SLP anomalies occurring over the Northern Hemisphere during the past century. *Allan* [2000] and *Tourre et al.* [2001] found these biennial, interannual, and decadal signals sharing similar patterns and evolution in covarying SST and SLP anomalies over the Global Ocean and Pacific Ocean, respectively. Yet subtle differences in these patterns suggest dynamical consequences. For example, the meridional scale of equatorial SST anomalies increases with increasing period scale, and the longitude location of maximum equatorial SST anomalies is displaced to the west with increasing period scale. These observations suggest that each quasiperiodic signal derives from a similar delayed action oscillator (DAO) model operating in the Pacific Basin, with only subtle differences separating them.

[3] *McCreary* [1983], *Zebiak and Cane* [1987], and *Schopf and Suarez* [1988] produced similar DAO models for the quasiperiodic behavior of El Niño in the Pacific Basin, resembling that described conceptually by *Graham and White* [1988] for the 1983 El Niño. In the latter descriptive study, warm SST anomalies in the eastern equatorial Pacific Ocean during El Niño were observed generating low SLP anomalies directly overhead in response to anomalous deep convection [*Graham and Barnett*, 1987]. They observed the latter generating westerly

[1]Scripps Institution of Oceanography, University of California San Diego, La Jolla, California, USA.
[2]LDEO of Columbia University, Palisades, New York, USA.
[3]Atmospheric and Environmental Research, Inc., Lexington, Massachusetts, USA.
[4]United States Geological Survey, San Diego, California, USA.

Copyright 2003 by the American Geophysical Union.
0148-0227/03/2002JC001490$09.00

zonal surface wind (ZSW) anomalies in the western/central equatorial ocean, as simulated by *Gill* [1980]. These westerly ZSW anomalies were found associated with off-equatorial cyclonic wind stress curl (WSC) anomalies, the latter observed to drive baroclinic Rossby waves near 10°N that take 12 to 18 months to propagate westward to the western maritime boundary of Asia. The incidence of off-equatorial Rossby waves on the western boundary were observed to reflect as equatorial Kelvin waves, the latter appearing to raise the depth of the pycnocline in the eastern equatorial Pacific Ocean. At about this time, *Battisti* [1988] determined that shallow equatorial Kelvin waves raised the pycnocline depth through their reflection as slower shallow equatorial Rossby waves at the eastern boundary. This sequence of cause-and-effect yields a delayed negative feedback that cools the warm SST anomalies in the eastern equatorial Pacific Ocean.

[4] Earlier, *White et al.* [1985a, 1986, 1987] and *Pazan et al.* [1986] had observed the reflection of off-equatorial Rossby waves during El Niño, recognizing its importance in altering pycnocline depth and SST in the eastern equatorial Pacific Ocean. Subsequently, this delayed negative feedback mechanism was observed operating during the 1987 El Niño [*White et al.*, 1989; *Kessler*, 1990]. Later, *White et al.* [1990] and *White and Tai* [1992] examined the Rossby wave reflection process in greater detail utilizing high-resolution sea level height (SLH) data from satellite altimetry, finding it generating both fast and slow equatorial waves, the slower waves coupled to the overlying atmosphere and propagating eastward along the equator with phase speeds of $\sim$0.30 m s^{-1}. These latter speeds are nearly an order of magnitude slower than those of the equatorial Kelvin waves (2.0 to 3.0 m s^{-1}).

[5] *Graham et al.* [1990] and *Graham and White* [1990] conducted experiments with the DAO model of *Zebiak and Cane* [1987], finding dominant off-equatorial Rossby waves of increasing latitude generating lower-frequency signals in the Pacific Basin similar to El Niño. This possibility was also recognized in the simulations of the DAO model by *Schopf and Suarez* [1988], recently confirmed in modeling studies of *Kirtman* [1997]. Subsequently, *Jacobs et al.* [1994] and *Zhang et al.* [1997] proposed that decadal and interdecadal variability in the Pacific Basin might be caused by a DAO model similar to that explaining El Niño but relying on the reflection of higher-latitude Rossby waves to produce the lower frequency variability. Indeed, evidence for this has been mounting. Recently, *Capotondi and Alexander* [2001a, 2001b] found decadal Rossby waves in the North Pacific Ocean, with peak amplitude near 15°N, driven there by westward propagating WSC anomalies in the northeast trade winds. They found the incidence of these decadal Rossby waves on the western boundary reflecting into both fast and slow waves traveling eastward along the equator.

[6] In the present study we examine anomalous SST, 18°C isotherm depth (Z18), upper ocean temperature (UOT), ZSW, meridional surface wind (MSW), WSC over the Pacific Basin from 1955 to 2000. These variables are taken from the reanalyses of ocean temperature [*White*, 1995] and atmosphere variables [*Kalnay et al.*, 1996]. We find the biennial, interannual, and decadal signals of *Tourre et al.* [2001] sharing a DAO model, with similarities and differences with the extant DAO model of *McCreary* [1983], *Zebiak and Cane* [1987], and *Schopf and Suarez* [1988]. First, we find each signal depending on wind-driven off-equatorial Rossby waves to provide the delayed-negative feedback to equatorial SST anomalies, with the different Rossby wave signals forced at different latitudes. This is consistent with observations on interannual period scales by *Graham and White* [1988], *Kessler* [1990], and *White and Tai* [1992]. Second, we find the incidence of off-equatorial Rossby waves on the western boundary reflecting as slow eastward propagating equatorial coupled waves, the latter dominating the fast equatorial Kelvin waves. The intrinsic amplification of these slow equatorial coupled waves appears to provide the delayed-negative feedback to SST anomalies in the central/eastern ocean. The latter introduces an additional delay in the extant DAO model while increasing the ratio of reflected-to-incident wave amplitude at the western boundary.

[7] Here we find the slow eastward propagating equatorial coupled waves to be consistent with those predicted by *Hirst* [1986], *Neelin* [1991], *Wang and Weisberg* [1994], and others. In related studies, the off-equatorial Rossby waves appear to be coupled to the overlying atmosphere as well, not only on biennial and interannual period scales [*Meyers*, 1979; *White et al.*, 1985b; *Kessler*, 1990; *White et al.*, 1998; *White*, 2000a] but possibly on decadal period scales [*Capotondi and Alexander*, 2001a, 2001b]. These observations call into question the reliance of the extant DAO model [e.g., *Zebiak and Cane*, 1987] on the linear interaction of wind-driven oceanic Rossby waves and equatorial Kelvin waves. Indeed, *Wang and Weisberg* [1994] found equatorial coupled Rossby waves and Kelvin waves to have slower phase speeds and larger meridional space scales than their uncoupled counterparts. Yet it may be even more complicated than that.

[8] In the present study we construct a modified DAO model, demonstrating how the various mechanisms and the size and sources of their delays yield the resulting frequencies of biennial, interannual, and decadal signals in the Pacific Basin. This differs from the extant DAO model [e.g., *Zebiak and Cane*, 1987] principally through differences in the western boundary reflection process and the subsequent generation of slow coupled waves traveling eastward along the equator, yielding additional delays in the system. We find the observed difference between the phase speeds of incident off-equatorial Rossby waves entering the western boundary and their apparent reflection into slow equatorial coupled waves to be much less than the phase speed difference between off-equatorial Rossby waves and their reflection into fast equatorial Kelvin waves. Thus the amplitude of incident off-equatorial Rossby waves are nominally maintained as they reflect into slow-coupled waves on the equator, as observed previously by *Kessler* [1990], *White and Tai* [1992], and *Capotondi and Alexander* [2001a, 2001b].

2. Data and Methods

[9] In this study we utilize six variables from two sources over the 45 years from 1955 to 2000. They are monthly ZSW, MSW, and WSC from the National Centers for Environmental Prediction and National Center for Atmospheric Research (NCEP/NCAR) reanalysis [*Kalnay et al.*, 1996]. Over the ocean the NCEP/NCAR reanalysis is based

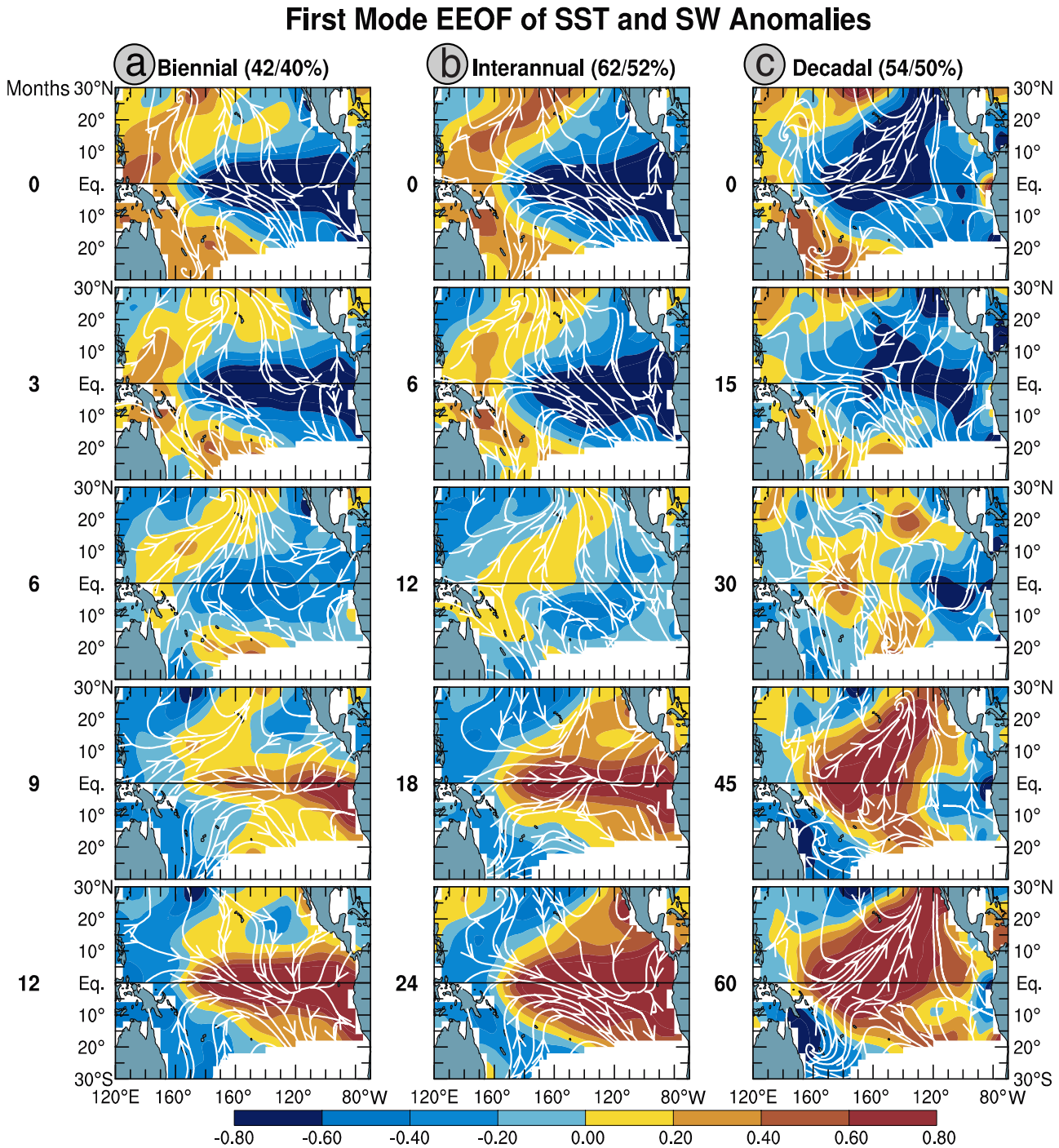

Figure 1a. Lag sequences of maps for the dominant mode in the EEOF analysis of SST and SW anomalies on (a) biennial, (b) interannual, and (c) decadal period scales. Each map extends over the Pacific Basin from 30°S–30°N. Each lag sequence extends from the tropical cool SST phase in the first lag-map to the tropical warm SST phase in the fifth lag-map, extending over one half cycle of variability on each period scale (that is, 12 months, 24 months, 60 months on biennial, interannual, and decadal period scales, respectively). The sense of propagation comes from following weights of similar sign or direction from one map to the next in each lag sequence. Yellow-to-red (blue) colors indicate warm (cool) SST weights; streamlines are parallel to SW vector weights. The color bar at the bottom ranges over ±0.8 standard deviations. Magnitude is given by the time sequences of amplitude (Figure 1b).

on the Comprehensive Ocean-Atmosphere Data Set (COADS) surface marine weather observations [*Slutz et al.*, 1985], the Reynolds' sea surface temperature (SST) analysis [*Reynolds and Marsico*, 1993], and atmospheric soundings from weather ships and satellites [*Kalnay et al.*, 1996]. We also utilize SST, UOT from the 0 to 400 m depth, and the 18°C isotherm depth (Z18) constructed each month from 1955 to 2000 using the Scripps Institution of Ocean-

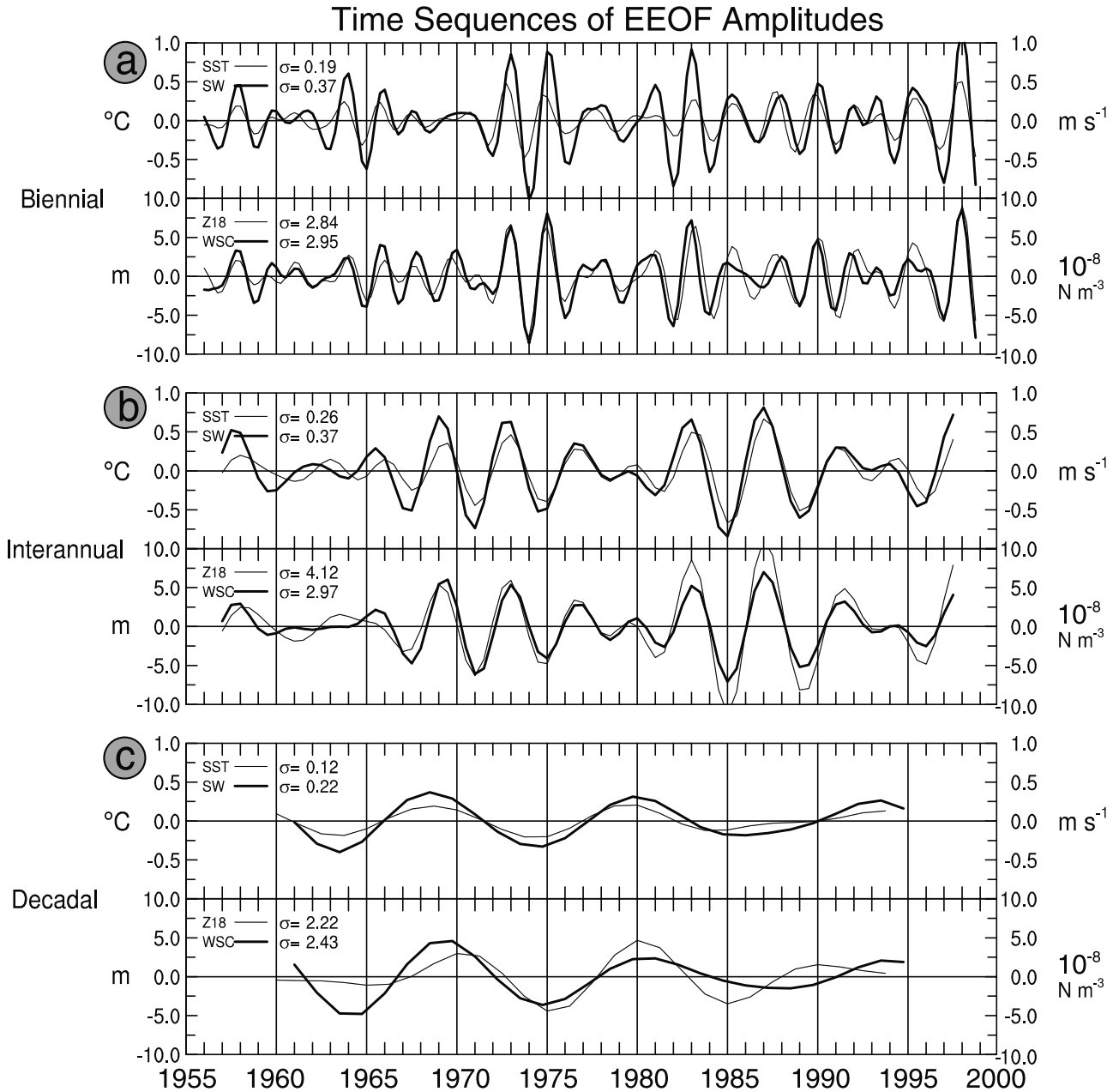

Figure 1b. Time sequences of amplitudes modulating the dominant lag sequences in the EEOF analysis of SST, SW, Z18, and WSC anomalies for 45 years from 1955 to 2000 on (a) biennial, (b) interannual, and (c) decadal period scales (see section 2). Dominant EEOF modes account for 42%/40%/33%/25%, 62%/52%/58%/38%, and 54%/50%/47%/51% of the variance for SST/SW/Z18/WSC anomalies on biennial, interannual, and decadal period scales, respectively. EEOF analysis was applied to SST, SW, Z18, and WSC anomalies independently on each period scale. The ordinate gives the amplitude of the signal, with the standard deviation (σ) given in each panel.

ography (SIO) upper ocean temperature reanalysis [*White*, 1995; *White et al.*, 2001]. The SIO reanalysis is based on all temperature profiles available at the National Oceanographic Data Center (NODC) [*Levitus et al.*, 1998a, 1998b].

[10] The observation of relatively narrow-band biennial, interannual, and decadal signals in the Pacific SST and SLP data sets over the 20th century [*Allan*, 2000; *White and Cayan*, 2000; *Tourre et al.*, 2001] at 2.2-, 2.8-, 3.5-, 5.4-, 7-, and 11-year periods allows us to isolate each of these signals and analyze them independently from each other. Thus we band-pass filter the time sequences of monthly anomalies from 1955 to 2000 using a period admittance window with half-power points at 1.5 to 3 years, 3 and 7 years, and 7 to 14 years, respectively [*Kaylor*, 1977]. Prior to band-pass filtering, we applied maximum entropy spectral analysis [*Andersen*, 1974] to reduce loss of data at the ends of each 45-year time sequence due to high-pass filtering and to preserve the integrity of the frequency response function of the filter. Thus maximum entropy spectral coefficients were used to extend the time sequences by an amount equal to half

the filter width on both ends of the record. This extension allows the half-power point criterion to be preserved in the frequency response function, and it allows over half the variance of the signal at the end points to be faithfully represented [*White*, 2000]. Since the filter response function of *Kaylor* [1977] is flat, with steep sides and negligible side lobes, the narrow-band decadal signal near 11-year period is effectively isolated from the narrow-band interannual signals at 5.4- and 3.5-year period, while the latter are effectively isolated from narrow-band biennial signals at 2.8- and 2.2-year period. On the other hand, the interannual signal at 7-year period is suppressed and its energy is smeared into the both the decadal and higher frequency interannual signals. Thus in subsequent analysis of the band-pass filtered interannual and decadal data, we must be aware of this potential source of cross-contamination.

[11] For the 45-year record, band-pass filtering yields ~22, ~11, and ~5 cycles of biennial, interannual, and decadal variability, respectively, with approximately 48, 24, and 12 effective temporal degrees of freedom [*Snedecor and Cochran*, 1980]. This filtering procedure reduces standard errors of filtered anomalies by factors of ~4, ~6, ~9, respectively, that is, the square root of independent monthly estimates in the low-pass portion of the band-pass filter.

[12] To illustrate the space-time evolution of biennial, interannual, and decadal signals, we apply extended empirical orthogonal function (EEOF) analysis [*Weare and Nasstrom*, 1982] to filtered SST, Z18, ZSW, MSW, and WSC anomalies over the Pacific Ocean from 30°S to 30°N. In EEOF analysis, each map of anomalous variability in the 45-year time sequence is replaced by a sequence of nine temporally lagged maps. These lag sequences yield the evolution of variability approximately over one full cycle of the signal, with the nine temporally lagged maps resolving the cycle in increments of ~45° of phase. Thus EEOF analysis yields time-lagged spatial sequences, which are modified by corresponding time sequences of amplitudes. In order to compare the EEOF lag sequences of one variable with that of another, we normalize them, giving them unit variance over the Pacific Basin, with magnitude carried by the time sequence of the amplitudes. The middle lag-map in each lag sequence can be multiplied by the time sequence of amplitudes to reveal its contribution to the original time sequence of anomaly maps. Here, we display only the first half cycle in each lag sequence (with five lag-maps describing ~180° of phase in the signal), adjusting the phase of each signal to visualize the canonical evolution from the tropical cool phase to the tropical warm phase. We conduct the EEOF analysis on the different variables independently, except for MSW and ZSW anomalies, the joint analysis of which yields the surface wind (SW) vector.

3. Covarying SST and SW Variability Over the Tropical Ocean

[13] An important mechanism within the extant DAO model has westerly ZSW anomalies in the western/central equatorial Pacific Ocean responding to warm SST anomalies in the central/eastern equatorial ocean as proposed by *Gill* [1980] and observed by *Graham and White* [1988] on interannual period scales. These ZSW anomalies are in ageostrophic balance with low SLP anomalies [*Ward and Hoskins*, 1996], which occur directly over the warm SST anomalies on each period scale [*Tourre et al.*, 2001] in response to the sensible-plus-latent heating of the overlying troposphere [*Graham and Barnett*, 1987]. To demonstrate that this occurs on biennial, interannual, and decadal period scales, we overlay lag sequences from the dominant first modes of the EEOF of SST and SW vector anomalies (Figure 1a). This superimposition is allowed because corresponding time sequences of EEOF amplitudes are similar on each period scale (Figure 1b).

[14] The first and last maps in these EEOF lag sequences (Figure 1a) describe the equatorial cool and warm phases, respectively. As such, these lag sequences yield the evolutionary development of covarying SST and SW variability during the 1/2 cycle leading up to peak equatorial warm phase. Keep in mind that the time sequences of amplitudes of dominant EEOF modes of SST and SW vector anomalies are aligned (Figure 1b) without having to force the issue by conducting a joint analysis. This is testament to the natural coupling of ocean and atmosphere variability occurring on all three period scales, consistent with that observed between SST and SLP anomalies by *Tourre et al.* [2001]. Moreover, the decadal and interannual signals can be seen to be relatively narrow band in these time sequences, indicating that potential cross-contamination from the overlap of interannual and decadal band-pass-filter frequency response functions (see section 2) is insignificant.

[15] The percentages of filtered variance over the 45-year record explained by these dominant SST (SW) EEOF modes are 42% (40%), 62% (52%), 54% (50%) for biennial, interannual, and decadal signals, respectively. Given independent samples of ~48, ~24, and ~12 for the three signals, respectively, the percentages of filtered variance explained by the first modes are significantly above those for the next most energetic modes of 10% (11%), 14% (14%), 28% (29%). This indicates that the first mode displays little or no mixing with the next most energetic mode [*North et al.*, 1982]. Even so, the decadal signal, with only four to five cycles sampled over the 45-year record, is only marginally resolved by the EEOF methodology.

[16] Inspecting the time sequences of amplitudes (Figure 1b) finds the strength of the decadal signal (with an SST standard deviation of ~0.12°C) to be 1/2-to-2/3 that of the interannual and biennial signals (with SST standard deviations of ~0.26°C and ~0.19°C, respectively). *White and Allan* [2001] found the amplitude of covarying SST and SLP signals on biennial period scales over the past 100 years modulated by the decadal signal, with amplitude weak during the decadal equatorial warm phase. Here we find a similar relationship. On biennial period scales, weak amplitudes in EEOF time sequences (a, Figure 1b) occurred during 1960, 1970, 1980, and 1992 when the decadal signal was in its tropical warm phase. This had an impact on the intensity of El Niño, since biennial signals were both robust and aligned with the interannual signal in 1958, 1973, 1983, 1992, and 1998, when El Niño was strongest.

[17] Now we focus on the covarying SST and SW lag sequences (Figure 1a). In the fifth lag-map in each sequence we find similar patterns of SST and SW variability for each signal. We find warm SST weights centered about the

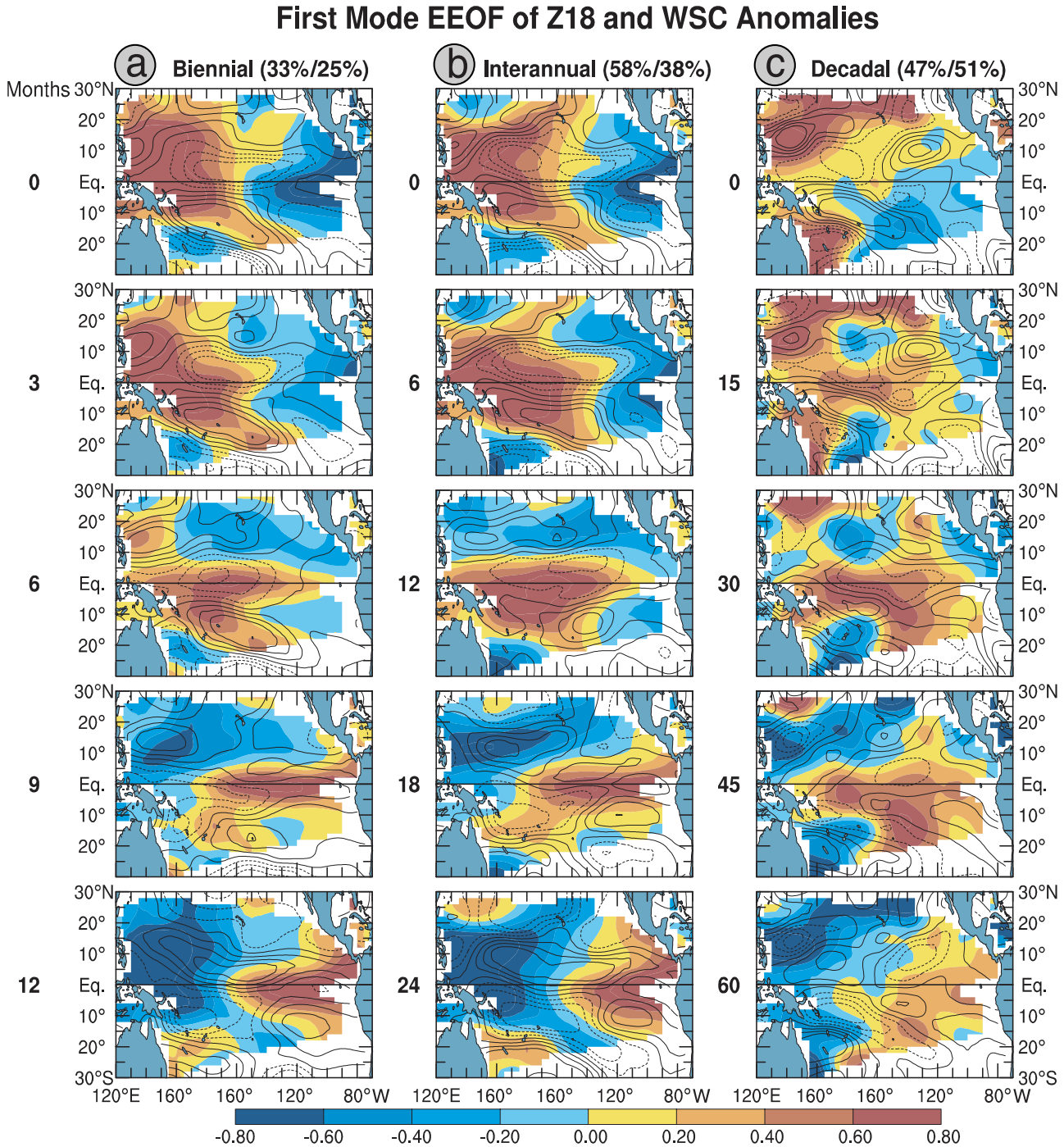

Figure 1c. Same as in Figure 1a, but for Z18 and WSC anomalies on (a) biennial, (b) interannual, and (c) decadal period scales, with yellow-to-red (blue) colors indicating deep (shallow) Z18 weights and solid (dashed) contours indicating positive (negative) WSC weights. The color bar at the bottom ranges over ±0.8 standard deviations. The contour interval of WSC weights is 0.2 standard deviations.

Figure 2a. (opposite) (top) The paths of the time-distance diagrams of Z18 anomalies in the North Pacific Ocean on biennial, interannual, and decadal period scales. (bottom) Time-distance diagrams of Z18 anomalies extending along these paths for 30 years from 1970 to 2000 on biennial period scales (a) and for 45 years from 1955 to 2000 on interannual period scales (b) and decadal period scales (c). Negative (positive) anomalies are hatched (unhatched). Sloping black lines and sloping dashed lines highlight the continuity of westward-propagating Rossby waves off the equator with eastward propagating coupled waves on the equator, respectively. Contours intervals are 5.0 m.

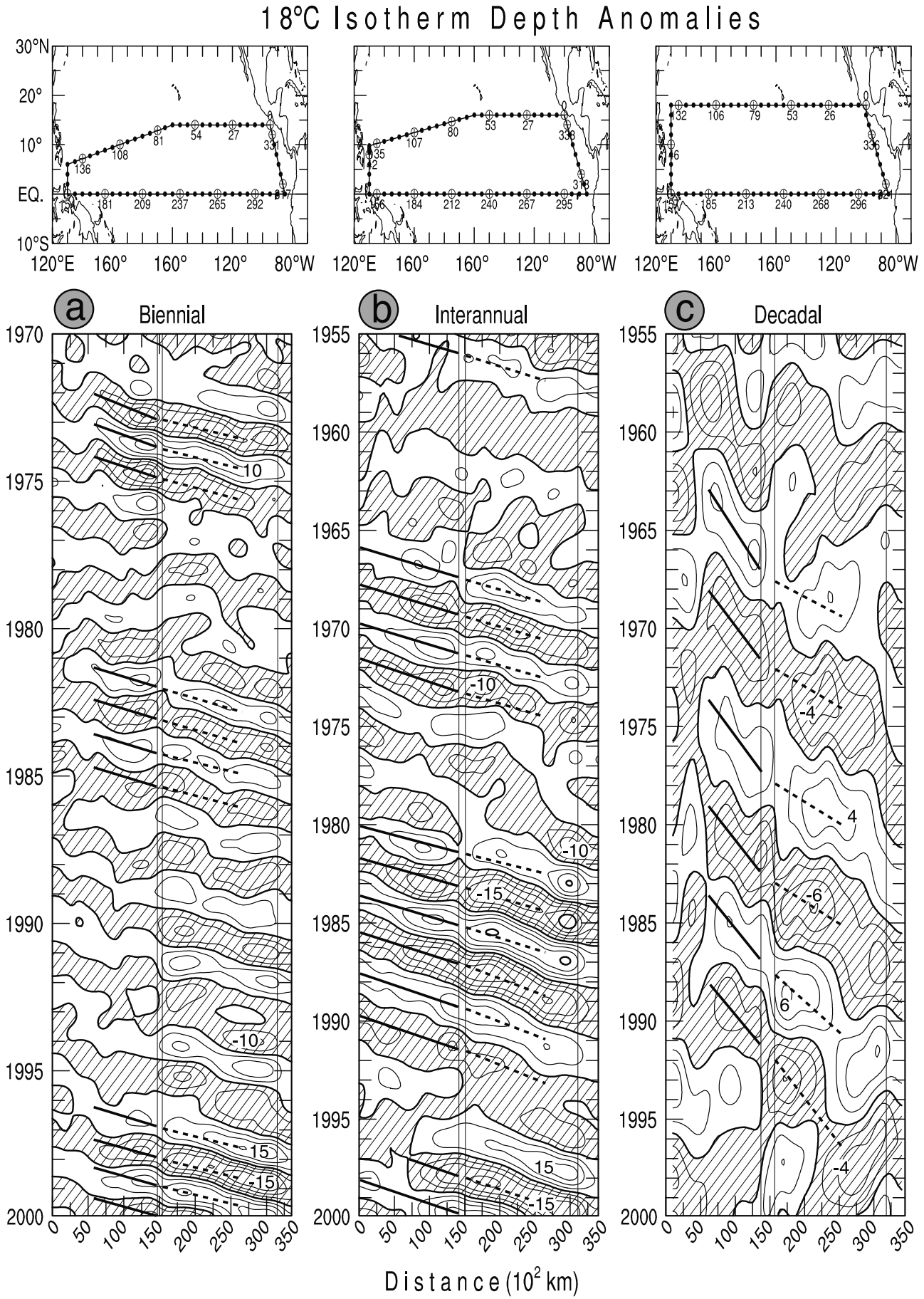
18°C Isotherm Depth Anomalies
30°N
20°
10°
EQ.
10°S
120°E 160° 160° 120° 80°W
a Biennial
b Interannual
c Decadal
1970 1975 1980 1985 1990 1995 2000
1955 1960 1965 1970 1975 1980 1985 1990 1995 2000
0 50 100 150 200 250 300 350
Distance (10^2 km)

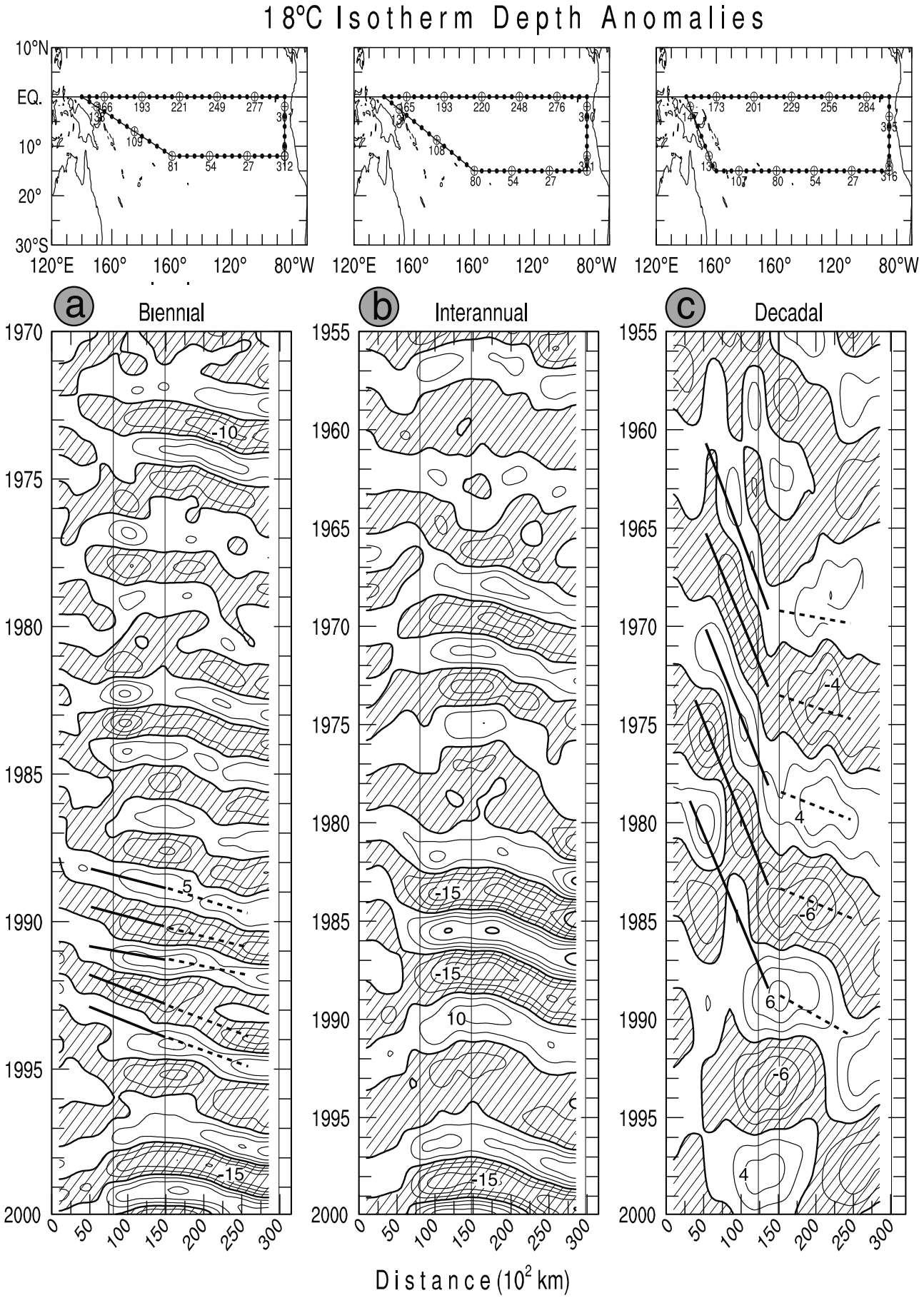

Figure 2b. Same as Figure 2a but for the South Pacific Ocean.

equator in the central/eastern equatorial ocean, associated with westward and equatorward SW vector weights in the western/central tropical ocean on each period scale. Yet in the central/eastern tropical ocean, the SW vector weights are directed southward from the Northern Hemisphere to the Southern Hemisphere on biennial and interannual period scales, while directed poleward (i.e., away from the equator) on decadal period scales. Thus the SW vector weights on biennial and interannual period scales over the entire Pacific basin are directed principally toward the anomalous low pressure node of the Southern Oscillation near Tahiti [*Berlage*, 1957], while on decadal period scales they are directed, to be sure, around the low pressure node of the Southern Oscillation near Tahiti but also around another node forming northeast of Hawaii, as observed by *Tourre et al.* [2001].

[18] Principal differences between the three signals in Figure 1a are the increase in the meridional scale of equatorial SST weights with increasing period scale and the increase in the longitude of maximum equatorial SST weights with increasing period scale, as observed by *Tourre et al.* [2001]. Here we also find zonal SW weights near the equator increasing their meridional scale with increasing period scale. As such, the decadal signal has maximum equatorial SST variability near 160°W, extending poleward into the eastern subtropical ocean in both hemispheres, the latter associated with off-equatorial poleward SW weights. These poleward SW weights yield cyclonic WSC weights in the central ocean extending from the equator into the subtropics in both hemispheres.

[19] On all three period scales, SW vector weights are directed toward (away from) warm (cool) SST scalar weights throughout most of the equatorial domain, transitioning to poleward (equatorward) SW vector weights over warm (cool) SST weights in the extraequatorial domain. In the fourth and fifth lag-maps (Figure 1a), the transition from primarily westerly ZSW weights in the western/central equatorial ocean to primarily poleward MSW weights off the equator in the central/eastern ocean (the latter aligned with warm SST weights) produces cyclonic WSC weights off the equator in both hemispheres, centered near the transition.

4. Wind-Driven Off-Equatorial Rossby Waves

[20] We seek evidence for wind-driven off-equatorial Rossby wave activity by examining lag sequences of the first EEOF mode of Z18 and WSC anomalies for biennial, interannual, and decadal signals (Figure 1c). As with SST and SW vector lag sequences (Figure 1a), Z18 and WSC lag sequences can be superimposed because corresponding time sequences of amplitudes are aligned (Figure 1b). Moreover, they are aligned with those of SST and SW vector anomalies (Figure 1b), indicating that the entire baroclinic structure of the upper ocean and lower troposphere fluctuates together naturally on the three period scales.

[21] The percentages of filtered variance explained over the 45-year record by these dominant Z18 (WSC) EEOF modes are 33% (25%), 58% (38%), 47% (51%) for biennial, interannual, and decadal signals, respectively, similar to those of dominant SST (SW) EEOF modes. These percentages of filtered variance explained are significantly above those of the next most energetic modes of 12% (10%), 13% (15%), 27% (28%), indicating that the first mode on each period scale displays little or no mixing with the next most energetic mode [*North et al.*, 1982].

[22] We restrict our description of the wind-driven off-equatorial Rossby waves in Z18 weights (Figure 1c) to the Northern Hemisphere, where Rossby waves on all three period scales are observed. In the second lag-map, shallow Z18 weights (blue colors, Figure 1c) on biennial and interannual period scales extend from 0° to 25°N in the eastern tropical ocean (i.e., east of 160°W), while on decadal period scales they extend from 10°N and 25°N latitude near the dateline. Subsequently, shallow Z18 weights can be seen propagating westward toward the maritime western boundary, reaching it by the fourth lag-map (Figure 1c). In the fourth lag-map, maximum shallow Z18 weights along the maritime western boundary occur farther north with increasing period scale; i.e., located between 3°N and 9°N, 5°N and 15°N, and 7°N and 18°N on biennial, interannual, and decadal period scales, respectively. Then, in the fifth lag-map (Figure 1c) the reflection process can be seen transmitting the off-equatorial signals onto the equator in the western equatorial ocean on all three period scales.

[23] So, as warm equatorial SST weights propagates slowly eastward over the second half of the lag sequence (Figure 1a), the associated westerly SW vector weights on the equator spawn cyclonic (positive) WSC weights off the equator in the western/central tropical ocean on all three period scales (Figure 1c), where they can be seen to pump the off-equatorial Rossby waves. In the third lag-map, with warm SST weights on the equator located principally in the western/central ocean (Figure 1a), the cyclonic WSC weights (Figure 1c) occur between 5°N and 25°N across the western/central tropical ocean on biennial and interannual period scales but are confined to the central tropical ocean between 10°N and 25°N on decadal period scales. These cyclonic WSC weights are responsible for the intensification of shallow off-equatorial Rossby waves appearing in Z18 weights in the fourth lag-month over this latitude domain on all three period scales. Moreover, it is in this fourth lag-map that the latitude of incidence of the negative Z18 weights (i.e., the shallow Rossby waves) upon the western boundary for each of the three signals is differentiated (Figure 1c), i.e., increasing with period scale as has already been described. Subsequently, in the fourth lag-month, when warm SST weights first appear in the eastern/central equatorial ocean (Figure 1a), the cyclonic WSC weights (Figure 1c) are displaced equatorward between 0° and 20°N across the entire tropical ocean on biennial and interannual period scales but again confined to the central/western ocean between 10°N and 20°N on decadal period scales. These cyclonic WSC weights can be expected to pump the shallow Z18 weights in the fifth lag-month over this latitude domain on all three period scales.

5. Slow Western Boundary Reflection of Incident Off-Equatorial Rossby Waves

[24] Now we begin the description of the Rossby wave reflection process of biennial, interannual, and decadal signals by focusing on the EEOF lag sequences of Z18

weights in the western/central tropical Pacific Ocean (Figure 1c). In the Northern Hemisphere during the second lag-map (Figure 1c), shallow Z18 weights can be seen in the eastern/central ocean between 10° and 20°N on all three period scales. By the fourth lag-map, these shallow Z18 weights have propagated westward across the tropical North Pacific Ocean to the western boundary, where they intensify between 5°N and 25°N and begin reflecting onto the equator. By the fifth lag-map, the reflection of these incident waves is well underway, indicated by the slow eastward phase propagation of shallow Z18 weights away from the western boundary along the equator.

[25] In the Southern Hemisphere during the second lag-map (Figure 1c), shallow Z18 weights occur between 0° and 20°S east of Tahiti on biennial and interannual period scales but not on decadal period scales. By the third lag-map, the shallow Z18 weights on biennial and interannual period scales begin disappearing, with the shallow Z18 weights on decadal period scales appearing between 10°S to 25°S west of Tahiti, symmetric about the equator with that forming in the Northern Hemisphere. By the fourth lag-map, the shallow Z18 weights on biennial and interannual period scales have effectively disappeared, with the shallow Z18 weights on decadal period scales propagating westward to the east coast of Australia. This evolutionary development reveals a fundamental difference between off-equatorial Rossby wave development in Northern and Southern Hemispheres on biennial and interannual period scales; i.e., the latter are absent in the Southern Hemisphere. This may be due to interference by the slow eastward phase propagation of covarying SST and SLP anomalies associated with the Southern Oscillation in the Southern Hemisphere [*White and Cayan*, 2000; *White and Allan*, 2001]. On the other hand, off-equatorial Rossby waves on decadal period scales can be seen developing symmetrically about the equator in both hemispheres.

[26] To examine this reflection process in greater detail, we construct time-distance diagrams around a circuit on each period scale in both the Northern and Southern Hemispheres (Figures 2a and 2b). These circuits follows the paths of off-equatorial Rossby waves westward across the tropical Pacific Ocean from the eastern boundary to the maritime western boundary of Austral-Asia; then they follow equatorial coupled waves eastward along on the equator, the latter propagating slowly poleward along the eastern boundary to the beginning of the circuit. To determine the path of off-equatorial Rossby waves, we follow the westward propagation of maximum Z18 weights over the latter half of the Z18 lag sequence (Figure 1c). This finds the mean path of dominant Rossby wave activity in the western tropical Pacific Ocean for biennial, interannual, and decadal signals ranging from 6°N to 13°N, 10°N to 16°N, and 18°N, respectively, in the Northern Hemisphere and 0° to 12°S, 0° to 15°S, and 15°S, respectively, in the Southern Hemisphere. To determine these paths more precisely, we determined the latitude whereby maximum continuity is achieved between off-equatorial Rossby waves incidence to the western boundary and equatorial coupled waves emanating from the western boundary, using trial and error. This procedure found the incidence of biennial, interannual, and decadal Rossby waves on the western boundary to be ~7°, ~12° and ~18°, respectively, in both hemispheres.

[27] In the Northern Hemisphere the reflection of off-equatorial Rossby waves at the western boundary on biennial, interannual, and decadal period scales (Figure 2a) was not always present during El Niño, as has been noted by *Picaut et al.* [1997]. On biennial period scales, the reflection was modulated by decadal change, with reflection restricted to the epochs from 1972 to 1975, 1981 to 1985, and 1996 to 1999 (a, Figure 2a). These are the same epochs defining the amplitude modulation of the biennial EEOF modes (Figure 1b). During these epochs, biennial Rossby waves were generated in the central tropical ocean by anomalous WSC forcing, taking ~6 months to propagate westward to the maritime western boundary of Asia where they reflect as slow equatorial coupled waves. On interannual period scales, reflection was modulated by interdecadal change, with reflection restricted to the epochs from 1966 to 1973, 1980 to 1992, and 1997 to 1999 (b, Figure 2a). These are the same epochs defining amplitude modulation of the interannual EEOF modes (Figure 1b). During these epochs, interannual Rossby waves were intensified in the western/central tropical ocean by anomalous WSC forcing, taking ~12 months to propagate westward to the maritime western boundary of Asia. From the late 1960s to early 1970s and during the 1980s the continuity of interannual Rossby waves with equatorial coupled waves and their extension poleward along the eastern boundary allowed the interannual signal to complete the entire circuit. Thus interannual Rossby waves in the eastern tropical ocean near 15°N derive from the slow poleward propagation of equatorial Z18 anomalies along the eastern boundary [*White*, 1994]. For decadal Rossby waves their western boundary reflection appears to be modulated by multidecadal change, with reflection occurring most clearly from 1967 to 1992 (c, Figure 2a). During this epoch, decadal Rossby waves were generated in the central/western tropical Pacific Ocean by anomalous WSC forcing, taking ~36 months to propagate westward to the maritime western boundary of Asia.

[28] In the Southern Hemisphere, western boundary reflection on biennial and interannual period scales (a and b, Figure 2b) was usually absent because the incident of off-equatorial Rossby waves on the western boundary near Australia was usually absent, as observed in the Z18 lag sequences (Figure 1c). On the other hand, westward phase propagation of decadal Rossby waves can be readily discerned (c, Figure 2b). These decadal off-equatorial Rossby waves were generated in the central tropical South Pacific Ocean west of Tahiti by anomalous WSC forcing, taking ~5 years to propagate westward to the western boundary at Australia. Since these Southern Hemisphere Rossby waves reflect onto the equator farther to the east than their Northern Hemisphere counterparts, we might have expected them to lead the latter in generating equatorial coupled wave activity. However, they did not; instead, they lagged the Northern Hemisphere Rossby wave reflection. Thus they do not display the same degree of continuity with the slow equatorial coupled waves in the time-distance diagrams.

[29] To demonstrate that the westward phase propagation of off-equatorial Z18 anomalies in Figure 2a and Figure 2b displays phase speeds similar to those of baroclinic Rossby waves, we estimate their celerity (Figure 3) from the average slope of tilted black lines given in the time-

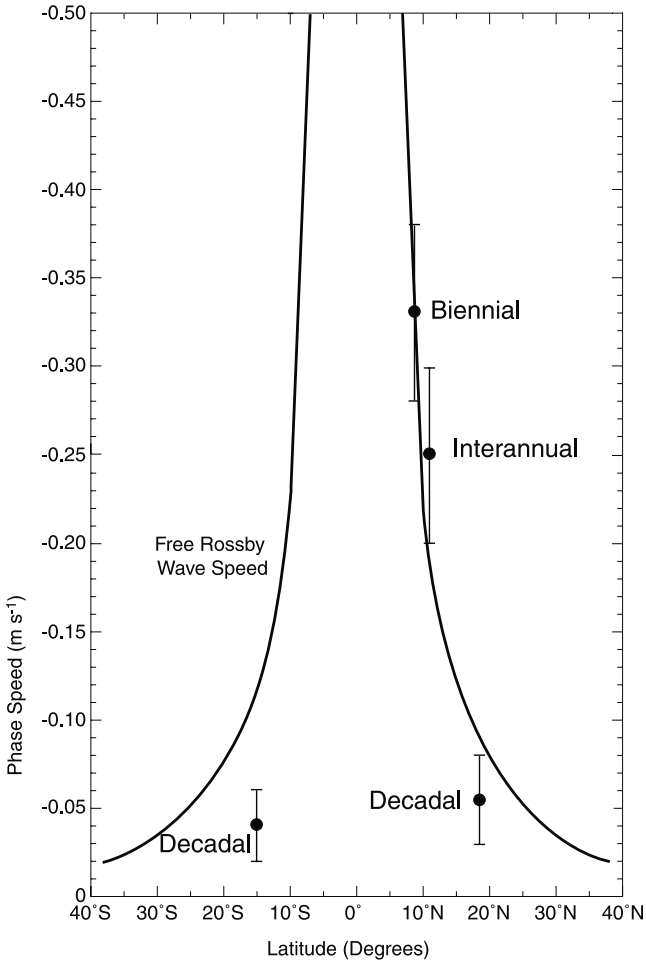

Figure 3. Meridional profile of theoretical first-mode baroclinic Rossby wave speeds [*Killworth et al.*, 1997] averaged across the Pacific Ocean from 20°S to 20°N together with observed zonal-average westward phase speeds for biennial, interannual, and decadal Rossby waves in the North Pacific Ocean and for decadal Rossby waves in the South Pacific Ocean. Observed phase speeds were estimated from the average of slopes given by the solid black lines in the time-distance diagrams of Z18 anomalies in Figure 2a and Figure 2b, with error bars representing the spread in these slopes.

longitude diagrams. Subsequently, we compare these zonal average phase speeds with those computed theoretically by *Killworth et al.* [1997]. The observed phase speeds are not significantly different from theoretical phase speeds on biennial and interannual period scales in the Northern Hemisphere, but they are significantly slower on decadal period scales in both hemispheres. This may occur because the decadal waves are coupled to the overlying atmosphere; however, this has yet to be demonstrated.

6. Eastward Phase Propagation of Slow Coupled Waves Along the Equator

[30] Earlier, *White and Allan* [2001] and *White and Cayan* [2000] observed covarying Z18 and ZSW anomalies on biennial and interannual period scales propagating slowly eastward along the equator in the Pacific Ocean in concert with global SST/SLP waves propagating slowly eastward across the tropical Indo-Pacific Ocean. The latter can be seen in the SST/SW lag sequences (a and b, Figure 1a). Here we find these covarying Z18 and ZSW anomalies either arising from, or coincident with, Rossby wave reflection at the maritime western boundary of the Pacific Basin. We leave for future study the relative influence of slow eastward global SST/SLP waves entering the Pacific Ocean from the Indian Ocean and the Rossby wave reflection at the western boundary of the Pacific Ocean. Here we focus attention on the covariance of Z18 and ZSW anomalies along the equator on biennial, interannual, and decadal period scales.

[31] We display time-longitude diagrams of ZI8 and ZSW anomalies along the equator (a, Figure 4), revealing the slow eastward phase propagation of coupled waves in covarying Z18 and ZSW anomalies for biennial, interannual, and decadal signals. We focus on those coupled waves occurring in response to Rossby wave reflection (Figure 2a, Figure 2b). This latter requirement finds the reflected equatorial coupled waves to be a subset of the total number on biennial and interannual period scales, with additional ones presumably generated in response to global SST/SLP waves entering the Pacific Ocean from the Indian Ocean [*White and Cayan*, 2000; *White and Allan*, 2001], consistent with *Picaut et al.* [1997]. Sloping black lines find covarying Z18 and ZSW anomalies aligned on all period scales, with slopes yielding eastward phase speeds of ~0.50, ~0.25, and ~0.12 m s^{-1} on biennial, interannual, and decadal period scales, respectively, taking ~6, ~12 and ~24 months to transit from the western boundary to the central/eastern equatorial ocean. The zonal-lag cross-correlation between Z18 and ZSW anomalies (b, Figure 4) finds westerly ZSW anomalies displaced to ~70° of phase to the west of covarying deep Z18 anomalies on all period scales, consistent with the quasi-stationary momentum balance between zonal surface wind stress and the zonal baroclinic pressure gradient [*White and Cayan*, 2000; *White and Allan*, 2001].

7. Superposition of Biennial, Interannual, and Decadal Signals During the 1992 El Niño

[32] Now we demonstrate the constructive interference of biennial, interannual, and decadal signals on the 1992 El Niño (Figure 5). On each period scale we display the evolution of positive UOT anomalies over the upper 400 m of ocean along a path extending westward off the equator from eastern boundary to western boundary, equatorward to the equator, then eastward along the equator back to the eastern boundary, and then poleward along that boundary, completing the circuit. On biennial, interannual, and decadal period scales, respectively, we show the evolution of the signal over the two years from 1989 to 1992, over the four years from 1987 to 1992, and over the 10 years from 1982 to 1992, in each case culminating at the beginning of the 1992 El Niño year.

[33] The animation sequence of the decadal signal from 1982 to 1992 (a, Figure 5) displays warm UOT anomalies generated at the depth of the main pycnocline near ~200 m about halfway between Hawaii and the western boundary (near the dateline) in 1983, taking ~3 years to propagate to the maritime boundary of Asia by 1986, where reflection

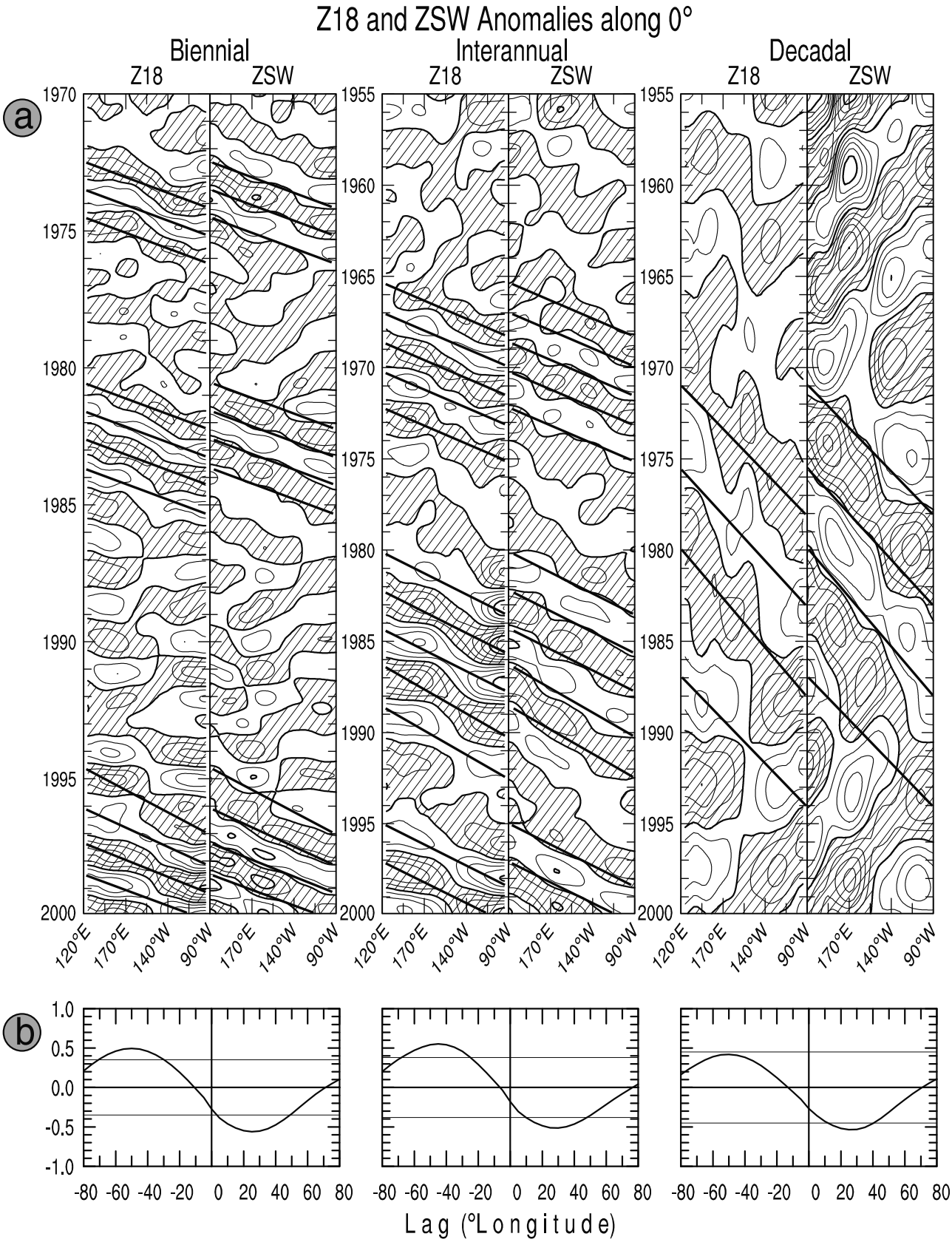
Z18 and ZSW Anomalies along 0°
Biennial
Interannual
Decadal
Z18
ZSW
a
b
1970
1975
1980
1985
1990
1995
2000
1955
1960
1965
120°E
170°E
140°W
90°W
1.0
0.5
0.0
-0.5
-1.0
-80 -60 -40 -20 0 20 40 60 80
Lag (°Longitude)

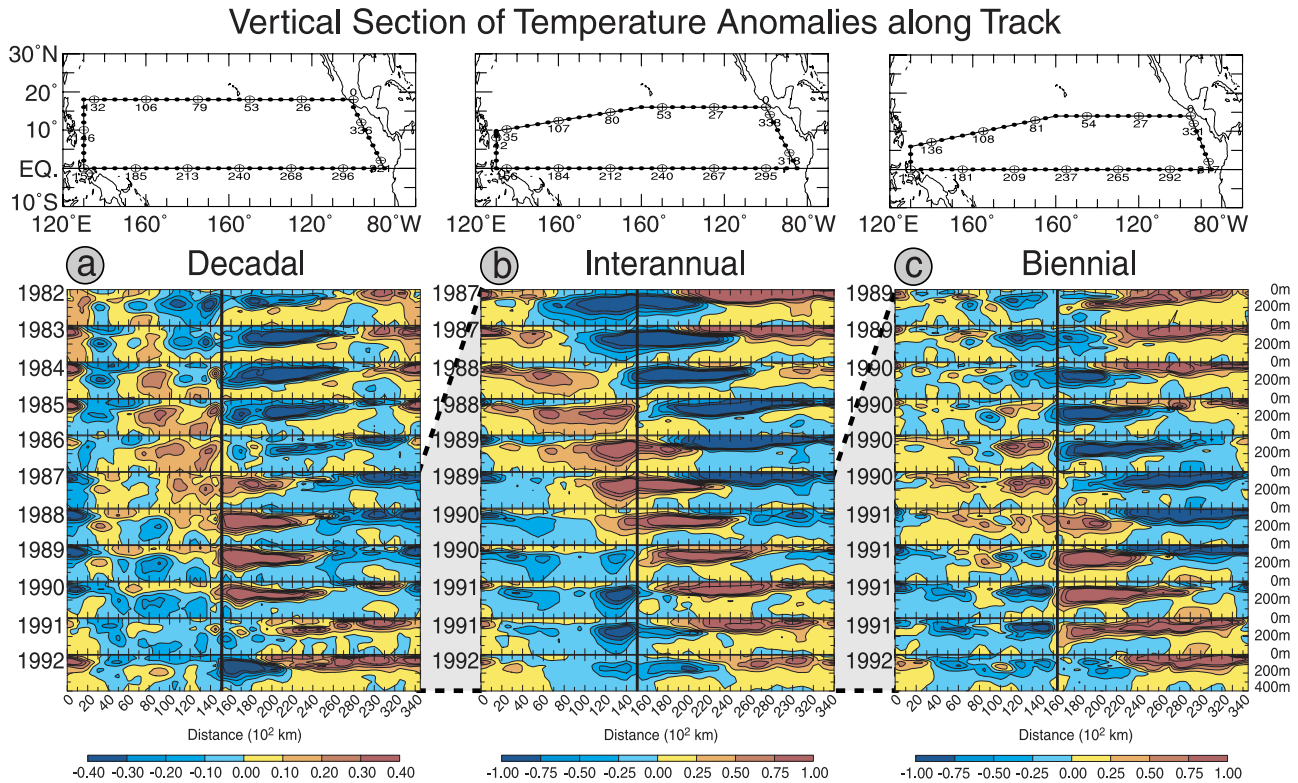

Figure 5. Animation sequences of vertical sections of upper ocean temperature (UOT) anomalies over the upper 400 meters along the path given at top, extending from the eastern boundary to the western boundary, onto the equator and back to the eastern boundary, making a complete circuit. The animation sequence for decadal UOT anomalies (a) extends from 1982 to 1992, while that for interannual UOT anomalies (b) extends from 1987 to 1992, while that for biennial UOT anomalies (c) extends from 1989 to 1992. Here we have embedded the biennial sequence within the interannual sequence and embedded the interannual sequence within the decadal sequence, allowing the reader to discern how the three signals interfere constructively with one another to enhance the 1992 El Niño event. Yellow-to-red (blue) colors indicate warm (cool) UOT anomalies, with contours indicating 0.10°C, 0.25°C, and 0.25°C intervals for decadal, interannual, and biennial signals, respectively.

can be seen occurring in 1987; thereafter, slow eastward phase propagation along the equator takes ~3 years to reach the central/eastern equatorial ocean in 1990. Superimposed on this decadal signal is an interannual signal (b, Figure 5) displaying warm UOT anomalies generated at the top of the main pycnocline at ~100 m depth southwest of Hawaii in 1987, taking ~12 months to propagate to the maritime boundary of Asia by 1988, where reflection can be seen occurring in 1989; thereafter, slow eastward phase propagation along the equator takes ~12 months to reach the central/eastern equatorial ocean in 1990. Finally, superimposed on these decadal and interannual signals is a biennial signal (c, Figure 5) displaying warm UOT anomalies generated at the top of the main pycnocline at ~100 m depth near the dateline during the middle of 1990, taking ~6 months to propagate to the western boundary by late 1990, where reflection can be seen during early 1991; thereafter, slow eastward phase propagation occuring along the equator takes ~6 months to reach the central/eastern equatorial ocean during late 1991. Thus during 1991 all three signals arrive in the central/eastern equatorial ocean in phase with one another to generate SST anomalies associated with the 1992 El Niño event.

8. A Conceptual Model of the DAO Paradigm

[34] We modify the extant DAO model, demonstrating how the various mechanisms and the size and sources of their delays yield the resulting frequency of each signal, similar to that given by *Graham and White* [1988]. This

Figure 4. (opposite) (a) Time-longitude diagrams of Z18 and ZSW anomalies along the equator in the Pacific Ocean. On biennial period scales the record extends over 30 years from 1970 to 2000, while for interannual and decadal period scales the record extends over 45 years from 1955 to 2000. Negative (positive) anomalies are hatched (unhatched). Sloping black lines allow the alignment of eastward phase propagation between the two variables to be seen on each period scale. Contours intervals are 5 m and 0.5 m s^{-1}, respectively. (b) Zonal-lag cross-correlations between Z18 and ZSW anomalies on biennial, interannual, and decadal period scales, with 90% confidence limits given by the horizontal dashed lines for 30, 24, and 12 effective degrees of freedom, respectively [*Snedecor and Cochran*, 1980].

model differs from that of *Graham and White* [1988] in two ways. First, the delay in the DAO is now due to the sum of those stemming from off-equatorial Rossby wave propagation from the western/central ocean to the western boundary and from the slow coupled wave propagation along the equator from the western boundary to the central/eastern equatorial ocean. These sums are ~12 months, ~24 months, and ~60 months on biennial, interannual, and decadal period scales, respectively. Second, the ratios of the amplitude of the reflected equatorial coupled wave to the amplitude of the incident off-equatorial Rossby wave in the DAO are ~1, ~1, and ~1/2 on biennial, interannual, and decadal period scales respectively. These amplitudes are much larger than those computed from linear Rossby wave/Kelvin wave theory.

[35] The conceptual coupled model is written as follows:

$$\mathrm{CZSW_t} = \mathrm{a\ ESST}_t + \varepsilon_t, \tag{1a}$$

$$\mathrm{CULT_{t+1}} = \mathrm{b\ CULT_t} - \mathrm{c\ CZSW_t}, \tag{1b}$$

$$\mathrm{WULT_t} = \mathrm{d\ CULT_{t+t1}}, \tag{1c}$$

$$\mathrm{ESST_t} = \mathrm{e(a)}^{-1}\mathrm{CZSW_t} + f\mathrm{WULT_{t+\tau 2}}. \tag{1d}$$

In equation (1a), ESST is the sea surface temperature anomaly in the central/eastern equatorial ocean, where "a" is 1.0 m s^{-1} per °C, and CZSW is the zonal surface wind anomaly in the western/central equatorial ocean, contemporaneous with and displaced to the west of ESST as observed in Figure 1a. In equation (1b), CULT is the upper layer thickness associated with the Rossby wave in the western/central off-equatorial ocean, pumped there by the anomalous wind stress curl, as observed in Figure 1c. The latter is considered contemporaneous with and proportional to the SST-induced CZSW in the western/central equatorial ocean, where "b" is 0.5 and "c" is 10.0 m per (m s^{-1}). In equation (1c), WULT is the upper layer thickness at the western boundary on the equator, which lags that of the Rossby wave pumped in the western/central off-equatorial ocean by a time-lag of $\tau 1$, where the amplitude ratio "d" is 1, 1, and 1/2 on biennial, interannual, and decadal period scales, as observed in Figure 2a. In equation (1d), $\tau 2$ is the time-lag for the upper layer thickness at the western boundary (WULT) to propagate to the central/eastern equatorial ocean, as observed in Figure 2a, where it influences the ESST presumably by altering the entrainment of cold water into the upper layer through wind mixing, where "f" is 0.1 °C per m and "e" is 0.25. The model is forced by white noise (ε_t) at time t in equation (1a), generating CZSW noise there which in turn generates CULT at time t+1 in equation (1b), which in turn generates WULT at a time t + 1 + $\tau 1$ in equation (1c), which in turn generates ESST at time t + 1 + $\tau 1$ + $\tau 2$ in equation (1d), which then feeds back into equation (1a) to influence CZSW at time t + 1 + $\tau 1$ + $\tau 2$, and so on.

[36] The tendency equations in this set are those of Ekman pumping and Rossby wave propagation in equations (1b) and (1c), respectively, and of equatorial coupled wave propagation in equation (1d). Dynamical equilibria occur in equations (1a) and (1d), on the one hand with warm SST-induced convection in the atmosphere driving westerly ZSW along the equator to the west (equation (1a)) and on the other hand with ZSW along the equator producing an immediate positive feedback to SST anomalies in the central/eastern ocean through its influence on the tilt of the main pycnocline along the equator (equation (1d)). This conceptual model produces a delayed negative feedback at a time lag of (1 + $\tau 1$ + $\tau 2$), since the CZSW in equation (1b) produces a CULT of opposite sign as the ESST. The magnitude of the response is dictated by coefficients "d" and "f", the former equal to the ratio of the reflected equatorial coupled wave amplitude to the incident off-equatorial Rossby wave amplitude, while the latter is the degree of influence that the wind-induced zonal tilt in the main pycnocline along the equator has on the SST anomalies in the central/eastern equatorial Pacific Ocean. Here "e" is chosen to be 0.25.

[37] The model is forced by stochastic variability in CZSW (i.e., ε_t in equation (1a)), with an RMS intensity of 0.1 m s^{-1}, with monthly time steps, producing a damped-resonant response near the period of 2 (1 + $\tau 1$ + $\tau 2$), similar to that obtained by *Graham and White* [1988]. We applied observed time lags and amplitude ratios on each period scale. This produces time sequences and spectra of ESST on each period scale (Figure 6). On biennial period scales (that is, with the model operated with an observed lag-sum of 12 months and amplitude ratio of 1), the model yields a spectrum (a, Figure 6) with a broad peak centered at a period of ~2.4 years. On interannual period scales (with an observed lag-sum of 24 months and amplitude ratio of 1), the model yields a spectrum (b, Figure 6) with a broad peak centered on a period of ~3.3 years. On decadal period scales (with an observed lag-sum of 60 months and amplitude ratio of 1/2), the model yields a spectrum (c, Figure 6) with a major peak centered at a period of ~11.0 years, with odd harmonics (i.e., T/3 and T/5) centered at periods of

Figure 6. (opposite) Time sequences of SST anomalies in the central/eastern equatorial Pacific Ocean, and their corresponding frequency power spectra, on (a) biennial, (b) interannual, and (c) decadal period scales simulated by the conceptual DAO model (equations (1a) through (1d)). The model results are differentiated by the sum of lags utilized in the model (i.e., 12 months, 24 months, and 60 months on biennial, interannual, and decadal period scales, respectively) and by the ratio of the amplitudes of incident to reflected waves at the western boundary (i.e., 1, 1, and 1/2 on biennial, interannual, and decadal period scales, respectively). On each period scale the model was driven for 25,000 years, so that the power spectra are highly resolved, with each spectral estimate having 200 degrees of freedom [*Bendat and Piersol*, 1986]. The model is forced by Gaussian-distributed white noise in the zonal surface wind field, with RMS variability of 0.1 m s^{-1} about zero mean, with the same noise (i.e., the same seed) used in the simulation on each period scale. This allows the time sequences on each period scale, taken over the same 50 years near the middle of the record, to be compared with one another.

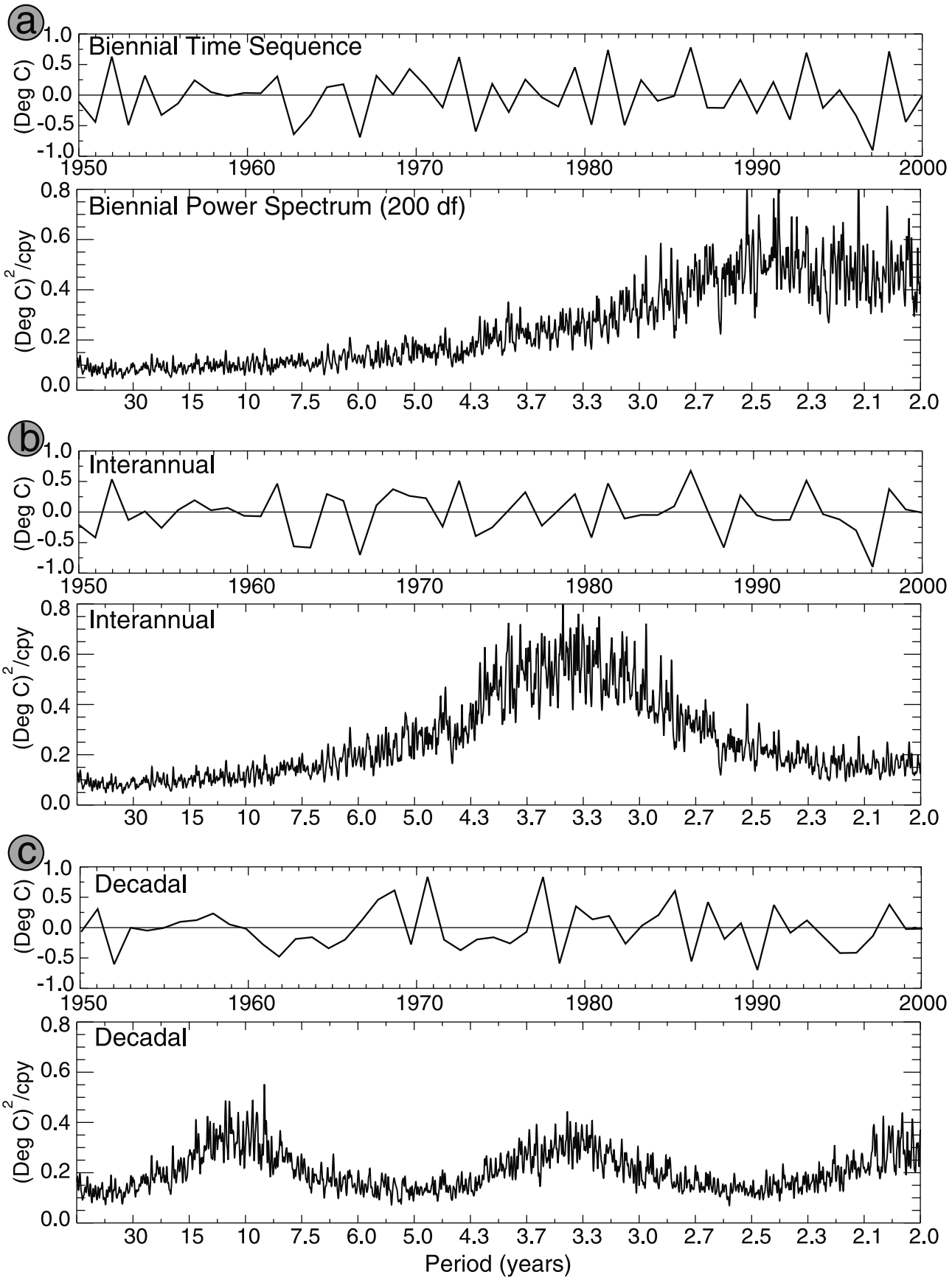
a
Biennial Time Sequence
(Deg C)
1.0
0.5
0.0
-0.5
-1.0
1950
1960
1970
1980
1990
2000
Biennial Power Spectrum (200 df)
(Deg C)^2/cpy
0.8
0.6
0.4
0.2
0.0
30
15
10
7.5
6.0
5.0
4.3
3.7
3.3
3.0
2.7
2.5
2.3
2.1
2.0
b
Interannual
(Deg C)
Interannual
(Deg C)^2/cpy
c
Decadal
(Deg C)
Decadal
(Deg C)^2/cpy
Period (years)

~3.4 years and ~2.1 years. These model signals are nearly as observed in the Pacific Ocean by *Tourre et al.* [2001]. Moreover, the time sequences of model biennial, interannual, and decadal signals (Figure 6) display magnitudes, which are consistent with those observed (i.e., ranging over ±1°C), with some evidence of amplitude and frequency modulation over the 50 years selected.

9. Discussion and Conclusions

[38] In the present study we find the biennial, interannual, and decadal signals in upper ocean temperature and winds in the Pacific Basin sharing patterns and evolution similar to those in the interannual DAO models of *McCreary* [1983], *Zebiak and Cane* [1987], *Schopf and Suarez* [1988] and *Graham and White* [1988]. The extant DAO model is the leading candidate for explaining the quasiperiodic behavior of El Niño [*Philander*, 1990]. Here we find it shared by biennial, interannual, and decadal signals, yet with significant differences. According to the extant DAO model, SST-induced wind-forced equatorial Rossby waves propagate westward to the maritime western boundary of Asia, where they reflect as Kelvin waves, which provide the delayed-negative feedback to SST anomalies in the eastern equatorial ocean. Here we find SST-induced wind-forced off-equatorial Rossby waves (not equatorial Rossby waves) propagating to the western boundary and reflecting as slow eastward propagating equatorial coupled waves. These equatorial coupled waves take as long to propagate eastward from the western boundary to the central/eastern ocean as it takes for the off-equatorial Rossby waves to propagate from the western/central ocean to the western boundary. Thus modification of the extant DAO model requires delays of similar magnitude stemming from both off-equatorial Rossby waves and slow equatorial coupled waves.

[39] The observed DAO model shared by biennial, interannual, and decadal signals differ from one another not in the mechanisms involved but in the phase speeds of off-equatorial Rossby waves and equatorial coupled waves on each period scale. The difference in Rossby wave speed stems from the latitude where these waves are generated by SST-induced off-equatorial wind stress forcing [*Graham et al.*, 1990], resulting in dominant off-equatorial Rossby waves at 7°N, 12°N, and 18°N on biennial, interannual, and decadal period scales, respectively. In the Southern Hemisphere this latitude is closer to 15°S for decadal signals, with biennial and interannual Rossby waves virtually absent, perhaps interfered with by eastward propagating signals in covarying SST and SLP anomalies [*White and Cayan*, 2000; *White and Allan*, 2001]. The difference in the latitude of anomalous SST-induced wind stress forcing of off equatorial Rossby waves in the Northern Hemisphere derives from the increase in meridional scale of equatorial SST anomalies (and corresponding equatorial zonal SW anomalies) with period scale. On the other hand, the difference in equatorial coupled wave speed probably depends upon the dynamics of coupling [e.g., *Hirst*, 1986; *Neelin*, 1991; *Wang and Weisberg*, 1994], which has yet to be differentiated among the three signals.

[40] Curiously, only the decadal Rossby waves are excited in both Northern and Southern Hemispheres, with biennial and interannual waves restricted to the Northern Hemisphere. These decadal Rossby waves are initiated by anomalous WSC forcing between 10° to 20°N from 160°W and 180° in the North Pacific Ocean and between 10° and 30°S from 160°W and 180° in the South Pacific Ocean. Initial development occurs ~90° of phase prior to the peak warm phase in the central/eastern equatorial ocean. Subsequently, the decadal Rossby waves are intensified by WSC forcing in the western/central off-equatorial ocean in association with the formation of ZSW anomalies on the equator leading up to peak equatorial warm and cool phases. In both hemispheres, the decadal off-equatorial Rossby waves travel slower than the theoretical Rossby phase speeds. This may occur because they are coupled to the overlying atmosphere, as has been observed on biennial and interannual period scales [*White et al.*, 1998; *White*, 2000a, 2000b].

[41] The interannual signal associated with El Niño has already been shown to be modulated by interdecadal variability by *Wang* [1995], *Balmaseda et al.* [1995], *Power et al.* [1999], *Torrence and Webster* [1999], and *White and Cayan* [2000]. And, the biennial signal has been shown to be modulated by decadal variability by *Allan* [2000] and *White and Allan* [2001]. Here we find off-equatorial Rossby wave activity and its reflection at the western boundary on biennial and interannual period scales to be modulated by decadal and interdecadal variability, respectively. Thus strong El Niño events of 1958, 1969, 1973, 1983, 1987, 1992, and 1998 occurred when interannual Rossby wave reflection was robust, while the weak El Niño events of 1963, 1965, 1976, 1979, and 1995 occurred when it was weak or absent. Moreover, the strongest El Niño events over the past 50 years (i.e., that in 1958, 1973, 1983, and 1998) occurred when the biennial and interannual signals were aligned with one another. Thus when the decadal signal was strong, the biennial signal was weak, and El Niños were weak. Earlier, *White and Allan* [2001] and *White and Cayan* [2000] found biennial and interannual signals to be weak (strong) in Niño-3 indices when the slow eastward phase propagation of the global SST/SLP waves was weak (strong). It remains to establish the connection between strong (weak) off-equatorial Rossby wave activity in the Northern Hemisphere and strong (weak) global SST/SLP waves on both biennial and interannual period scales.

[42] We constructed a modified DAO model, demonstrating how the various mechanisms, and the size and sources of their delays, yield the resulting frequency of each signal. In this model, the net delay is the sum of those due to off-equatorial Rossby wave propagation from the western/central ocean to the western boundary and due to slow coupled wave propagation along the equator from the western boundary to the central/eastern equatorial ocean. This sum is observed to be ~12 months, ~24 months, and ~60 months for biennial, interannual, and decadal signals, respectively. In this model, the ratio of the amplitude of the reflected equatorial coupled wave to the amplitude of the incident off-equatorial Rossby wave was taken to be that observed; i.e., ~1, ~1, and ~1/2 for biennial, interannual, and decadal signals respectively. Subsequently, driving the DAO model with white noise in the equatorial wind field yields quasiperiodic biennial, interannual, and decadal signals with frequencies (i.e., corresponding to periods of 2.4

years, 3.3 years, and 11 years), similar to those observed by *Tourre et al.* [2001].

[43] In this DAO model, each signal requires the background noise to be the source of energy. Whether this is true of the observed biennial, interannual, and decadal signals in the Pacific basin remains to be determined. Yet the fact that observed biennial and interannual signals are modulated by the decadal and interdecadal signals, respectively [e.g., *White and Allan*, 2001; *White and Cayan*, 2000] suggests that the phasing of the DAO is more deterministic than simulated with the present model. The major question is why these particular biennial, interannual, and decadal signals, revealed by *Tourre et al.* [2001] for the Pacific ocean-atmosphere system and by *Allan* [2000] for the global ocean-atmosphere system, are excited above those in adjacent frequency bands.

[44] **Acknowledgments.** Appreciation is extended to Arthur (Ted) Walker, the programmer responsible for the analyses conducted in this study. We extend our thanks to Andrea Fincham who is responsible for drafting the figures displayed in this study. Warren White is supported by Office of Global Programs of NOAA (NOAA NA 17RJ1231) under the Experimental Climate Prediction Center and by the National Aeronautics and Space Administration (NASA) under contract JPL1205106. Warren White is also supported by the Scripps Institution of Oceanography of the University of California, San Diego. Matt Barlow is supported by the Atmospheric and Environmental Research, Inc. Michael Dettinger is supported by the United States Geological Survey. Yves Tourre is supported by LDEO at Columbia University and by Météo-France.

References

Allan, R. J., ENSO and climatic variability in the last 150 years, in *El Niño and the Southern Oscillation: Multiscale Variability, Global and Regional Impacts*, edited by H. F. Diaz and V. Markgraf, pp. 3–55, Cambridge Univ. Press, New York, 2000.

Andersen, N., On the calculation of filter coefficients for maximum entropy spectral analysis, *Geophysics*, *39*, 69–72, 1974.

Balmaseda, M. A., M. K. Davey, and D. L. T. Anderson, Decadal and seasonal dependence of ENSO prediction skill, *J. Clim.*, *8*, 2705–2715, 1995.

Battisti, D. S., Interannual variability in the tropical atmosphere-ocean models, in *Climate Ocean Dynamics*, edited by M. E. Schlesinger, Kluwer Acad., Norwell, Mass., 1988.

Bendat, J. S., and A. G. Piersol, *Random Data: Analysis and Measurement Procedures*, 566 pp., John Wiley, New York, 1986.

Berlage, H. P., Fluctuations of the general atmospheric circulation of more than one-year, their nature and prognostic value, *K. Ned. Meteorol. Inst. Meded. Verh., 69*, 152 pp., 1957.

Capotondi, A., and M. A. Alexander, The influence of thermocline topography on the oceanic response to fluctuating winds: A case study in the tropical North Pacific Ocean, in *Advances in Mathematical Modeling of Atmosphere and Ocean Dynamics*, edited by P. F. Hodnett, pp. 119–124, Kluwer Acad., Norwell, Mass., 2001a.

Capotondi, A., and M. A. Alexander, Rossby waves in the tropical North Pacific and their role in decadal thermocline variability, *J. Phys. Oceanogr.*, *31*, 3496–3515, 2001b.

Gill, A. E., *Atmosphere-Ocean Dynamics*, 662 pp., Academic, San Diego, Calif., 1980.

Graham, N. E., and T. P. Barnett, Sea surface temperature, surface wind divergence, and convection over tropical oceans, *Science*, *238*, 657–659, 1987.

Graham, N. E., and W. B. White, The El Niño cycle: A natural oscillator of the Pacific ocean-atmosphere system, *Science*, *240*, 1293–1302, 1988.

Graham, N. E., and W. B. White, The role of the western boundary in the ENSO cycle: Experiments with coupled models, *J. Phys. Oceanogr.*, *20*, 1935–1948, 1990.

Graham, N. E., W. B. White, and A. Pares-Sierra, Low frequency ocean-atmosphere interactions in the tropical Pacific, in *Air-Sea Interaction in the Tropical Western Pacific*, edited by C. Jiping and J. Young, pp. 457–484, China Ocean Press, Beijing, 1990.

Hirst, A. C., Slow instabilities in tropical ocean basin-global atmospheric models, *J. Atmos. Sci.*, *45*, 830–852, 1986.

Jacobs, G. A., H. E. Hurlburt, J. C. Kindle, E. J. Metzger, J. L. Mitchell, W. J. Teague, and A. J. Wallcraft, Decade-scale Trans-Pacific propagation and warming effects of an El Niño anomaly, *Nature*, *370*, 360–363, 1994.

Kalnay, E., et al., The NCEP/NCAR 40-year reanalysis project, *Bull. Am. Meteorol. Soc.*, *77*, 437–471, 1996.

Kaylor, R. E., Filtering and decimation of digital time series, *Tech Rep. Note BN 850*, 14 pp., Inst. Phys. Sci, and Tech., Univ. of Maryland, College Park, Md., 1977.

Kessler, W. S., Observation of long Rossby waves in the northern tropical Pacific, *J. Geophys. Res.*, *95*, 5219–5813, 1990.

Killworth, P. D., D. B. Chelton, and R. A. deZoeke, The speed of observed and theoretical long extra-tropical planetary waves, *J. Phys. Oceanogr.*, *27*, 1946–1966, 1997.

Lau, K.-M., and H. Weng, Climate signal detection using wavelet transform: How to make a time series sing, *Bull. Am. Meteorol. Soc.*, *76*, 2391–2402, 1995.

Levitus, S., T. P. Boyer, M. E. Conkright, T. O'Brien, J. Antonov, C. Stephens, L. Stathoplos, D. Johnson, and R. Gelfeld, *World Ocean Database 1998*, vol. 1, *Introduction*, NOAA Atlas NESDIS 18, U.S. Govt. Print. Off., Washington, D.C., 1998a.

Levitus, S., T. P. Boyer, M. E. Conkright, D. Johnson, T. O'Brien, J. Antonov, C. Stephens, and R. Gelfeld, *World Ocean Database 1998*, vol. 2, *Temporal Distribution of Mechanical Bathythermograph Profiles*, NOAA Atlas NESDIS 19, U.S. Govt. Print. Off., Washington, D.C., 1998b.

Mann, M. E., and J. Park, Joint spatio-temporal modes of surface temperature and sea level pressure variability in the Northern Hemisphere during the last century, *J. Clim.*, *9*, 2137–2162, 1996.

McCreary, J. P., A model of tropical ocean-atmosphere interaction, *Mon. Weather Rev.*, *111*, 370–387, 1983.

Meyers, G., On the annual Rossby wave in the tropical North Pacific Ocean, *J. Phys. Oceanogr.*, *9*, 663–674, 1979.

Neelin, J. D., The slow sea surface temperature mode and the fast-wave limit: Analytical theory for tropical interannual oscillations and experiments in a hybrid coupled model, *J. Atmos. Sci.*, *48*, 584–606, 1991.

North, G. R., T. L. Bell, R. F. Cahalan, and F. G. Moeng, Sampling errors in the estimation of empirical orthogonal functions, *Mon. Weather Rev.*, *110*, 699–706, 1982.

Pazan, S. E., W. B. White, M. Inoue, and J. J. O'Brien, Off-equatorial influence upon Pacific equatorial dynamic height variability during the 1982–83 El Niño/Southern Oscillation event, *J. Geophys. Res.*, *91*, 8437–8449, 1986.

Picaut, J., M. Ioualalen, C. Menkes, T. Delcroix, and M. J. McPhadden, Mechanisms for the zonal displacement of the Warm Pool, *Science*, *274*, 1486–1489, 1997.

Philander, S. G., *El Niño, La Niña, and the Southern Oscillation*, 293 pp., Academic, San Diego, Calif., 1990.

Power, S., T. Casey, C. Folland, A. Colman, and V. Mehta, Inter-decadal modulation of the impact of ENSO on Australia, *Clim. Dyn.*, *15*, 319–324, 1999.

Reynolds, R. W., and D. C. Marsico, An improved real-time global sea surface temperature analysis, *J. Clim.*, *6*, 114–119, 1993.

Schopf, P. S., and M. J. Suarez, Vacillations in a coupled ocean-atmosphere model, *J. Atmos. Sci.*, *45*, 549–566, 1988.

Slutz, R. J., S. J. Lubker, J. D. Hiscox, S. D. Woodruff, R. L. Jenne, D. H. Joseph, P. M. Steurer, and J. D. Elms, *Comprehensive Ocean-Atmosphere Data Set: Release 1*, 268 pp., NOAA Environ. Res. Lab., Boulder, Colo., 1985.

Snedecor, G. W., W. G. Cochran, *Statistical Methods*, 507 pp., Iowa State Univ. Press, Ames, Iowa, 1980.

Torrence, C., and P. J. Webster, Interdecadal changes in the ENSO-Monsoon system, *J. Clim.*, *12*, 2679–2690, 1999.

Tourre, Y. M., B. Rajagopalan, Y. Kushnir, M. Barlow, and W. B. White, Patterns of coherent decadal and interdecadal climate signals in the Pacific Basin during the 20th Century, *Geophys. Res. Lett.*, *28*, 2069–2072, 2001.

Ward, M. N., and B. J. Hoskins, Near surface winds over the global ocean 1949–1988, *J. Clim.*, *9*, 1877–1895, 1996.

Wang, B., Interdecadal changes in El Niño onset in the last four decades, *J. Clim.*, *8*, 267–285, 1995.

Wang, C., and R. H. Weisberg, On the "Slow Mode" mechanism in ENSO-related coupled ocean-atmosphere models, *J. Clim.*, *7*, 1657–1667, 1994.

Weare, B., and J. Nasstrom, Examples of extended empirical orthogonal function analysis, *Mon. Weather Rev.*, *110*, 481–485, 1982.

White, W. B., Slow El Niño-Southern oscillation boundary waves, *J. Geophys. Res.*, *99*, 22,737–22,751, 1994.

White, W. B., Design of a global observing system for gyre-scale upper ocean temperature variability, *Progr. Oceanogr.*, *36*, 169–217, 1995.

White, W. B., Influence of the Antarctic circumpolar wave on Australia precipitation from 1958–1997, *J. Clim.*, *13*, 2125–2141, 2000a.

White, W. B., Tropical coupled Rossby waves in the Pacific ocean-atmosphere system, *J. Clim.*, *30*, 1245–1264, 2000b.

White, W. B., and R. J. Allan, A global quasi-biennial wave in surface temperature and pressure and its decadal modulation from 1900 to 1994, *J. Geophys. Res.*, *106*, 26,789–26,803, 2001.

White, W. B., and D. R. Cayan, A global ENSO wave in surface temperature and pressure and its interdecadal modulation from 1900 to 1996, *J. Geophys. Res.*, *105*, 11,223–11,242, 2000.

White, W. B., and C.-K. Tai, Reflection of interannual Rossby waves at the maritime western boundary of the tropical Pacific, *J. Geophys. Res.*, *97*, 14,305–14,322, 1992.

White, W. B., G. Meyers, J. R. Donguy, and S. E. Pazan, Short-term climate variability in the thermal structure of the Pacific Ocean during 1979–1982, *J. Phys. Oceanogr.*, *15*, 1917–1935, 1985a.

White, W. B., S. Pazan, and B. Li, Processes of short-term climatic variability in the baroclinic structure of the interior Western Tropical North Pacific, *J. Phys. Oceanogr.*, *15*, 386–402, 1985b.

White, W. B., S. Pazan, M. Inoue, and J. J. O'Brien, Off-equatorial influence upon Pacific equatorial dynamic height variability during the 1982–83 El Niño/Southern Oscillation event, *J. Geophys. Res.*, *191*, 8437–8449, 1986.

White, W. B., S. Pazan, and M. Inoue, Hindcast/Forecast of ENSO events based upon the redistribution of observed and model heat content in the western North Pacific, 1984–86, *J. Phys. Oceanogr.*, *17*, 264–280, 1987.

White, W. B., Y.-H. He, and S. E. Pazan, Off-equatorial westward propagating Rossby waves in the tropical Pacific during the 1982–83 and 1986–87 ENSO events, *J. Phys. Oceanogr.*, *19*, 1397–1406, 1989.

White, W. B., N. Graham, and C.-K. Tai, Reflection of annual Rossby waves at the maritime western boundary of the tropical Pacific, *J. Geophys. Res.*, *95*, 3101–3116, 1990.

White, W. B., Y. Chao, and C.-K. Tai, Coupling of biennial oceanic Rossby waves with the overlying atmosphere in the Pacific basin, *J. Phys. Oceanogr.*, *28*, 1236–1251, 1998.

White, W. B., D. R. Cayan, M. Dettinger, and G. Auad, Sources of global warming in upper ocean temperature during El Niño, *J. Geophys. Res.*, *106*, 4349–4367, 2001.

Zebiak, S. E., and M. A. Cane, A model El Niño-Southern Oscillation, *Mon. Weather Rev.*, *115*, 2262–2278, 1987.

Zhang, J., W. Wallace, and D. S. Battisti, ENSO-like interdecadal variability: 1900–93, *J. Clim.*, *10*, 1004–1020, 1997.

M. Barlow, Atmospheric and Environmental Research, Inc., Lexington, MA 02421, USA. (mbarlow@aer.com)

M. Dettinger, United States Geological Survey, San Diego, CA 92123, USA. (mddettin@usgs.gov)

Y. M. Tourre, Yves M. Tourre LDEO of Columbia University, Palisades, New York, USA. (Yvestourre@aol.com)

W. B. White, Scripps Institution of Oceanography, University of California San Diego, La Jolla, CA 92093-0230, USA. (wbwhite@ucsd.edu)